

# Tight and loose shapes in flat entangled dense polymers

A. Hanke<sup>1,a</sup>, R. Metzler<sup>2,b</sup>, P.G. Dommersnes<sup>3</sup>, Y. Kantor<sup>4</sup>, and M. Kardar<sup>5</sup>

<sup>1</sup> Institut für Theoretische Physik, Universität Stuttgart, Pfaffenwaldring 57, D-70550 Stuttgart, Germany

<sup>2</sup> NORDITA, Blegdamsvej 17, DK-2100 Copenhagen Ø, Denmark

<sup>3</sup> Institut Curie, 11 rue Pierre et Marie Curie, F-75231 Paris Cedex 5, France

<sup>4</sup> School of Physics and Astronomy, Raymond and Beverly Sackler Faculty of Exact Sciences, Tel Aviv University, Tel Aviv 69978, Israel

<sup>5</sup> Department of Physics, Massachusetts Institute of Technology, Cambridge, MA 02139, USA

Received 24 July 2003 and Received in final form 7 October 2003 /

Published online: 21 November 2003 – © EDP Sciences / Società Italiana di Fisica / Springer-Verlag 2003

**Abstract.** We investigate the effects of topological constraints (entanglements) on two-dimensional polymer loops in the dense phase, and at the collapse transition ( $\Theta$ -point). Previous studies have shown that in the dilute phase the entangled region becomes tight, and is thus localised on a small portion of the polymer. We find that the entropic force favouring tightness is considerably weaker in dense polymers. While the simple figure-eight structure, created by a single crossing in the polymer loop, localises weakly, the trefoil knot and all other prime knots are loosely spread out over the entire chain. In both the dense and  $\Theta$  conditions, the uncontracted-knot configuration is the most likely shape within a scaling analysis. By contrast, a strongly localised figure-eight is the most likely shape for dilute prime knots. Our findings are compared to recent simulations.

**PACS.** 87.15.-v Biomolecules: structure and physical properties – 82.35.-x Polymers: properties; reactions; polymerization – 02.10.Kn Knot theory

## 1 Introduction

Knots, and topological constraints in general, play an important role in macromolecular systems. In gels and rubbers, permanent entanglements strongly influence the equilibrium and relaxation properties [1–4]. Even single molecules with identical chemical structure but different topology may exhibit different physical properties [5]. Knots are also present in biological molecules: For example, some proteins exhibit knotted configurations [6], and the active modification of DNA knots through energy-consuming enzymes (topoisomerases) poses interesting challenges to the issue of the knot detection [7,8]. Experimentally, the observation of individual molecules by single-molecule force spectroscopy has come of age [9,10]; these methods can be used to probe the mechanical behaviour of knotted biopolymers directly.

Given a knot in a closed ring, an obvious question is whether, on average, the knot segregates into a small region in which all topological details are confined, and a large, simply connected segment; or whether it is loosely spread over the entire chain. In the dilute phase, it has been found by numerical evidence that flattened (hence

two-dimensional [11]) knots are localised, *i.e.* *tight* [12]. In a previous study [13], we developed an analytical approach, based on scaling results for polymer networks [14, 15], which explains and quantifies the tightness of any prime knot in flat (2D) dilute polymer loops. Some aspects of our results have been verified experimentally by means of a vibrated granular chain [16]. It should be mentioned that DNA chains have experimentally been flattened by adsorption on an adhesive membrane [17]. In 3D, the global topological constraints of a knot are hard to implement by analytical methods [18]. (A simpler topological invariant, the linking number of closed DNA rings, can be incorporated in the mapping to a field theory [1] by means of suitable gauge fields [19].) Consequently, the tightness or localisation of 3D knots has not been conclusively characterised. A number of phenomenological models and numerical studies support the localisation of simple knots [20]. Tightness has also been found in 3D slip-linked polymer chains in the dilute phase [21]. Conversely, delocalisation has been predicted for more complicated knots [22].

In many situations, however, polymer chains are not dilute. Polymer melts, gels, or rubbers exhibit fairly high densities of chains, and the behaviour of an individual chain in such systems is significantly different compared

<sup>a</sup> e-mail: hanke@theo2.physik.uni-stuttgart.de

<sup>b</sup> e-mail: metz@nordita.dk

to the dilute phase [1,2]. Similar considerations apply to biomolecules: In bacteria, the gyration radius of the almost freely floating ring DNA is often larger than the cell radius itself. Moreover, under certain conditions, there is a non-negligible osmotic pressure due to vicinal layers of protein molecules, which tends to confine the DNA [23]. In protein-folding studies, globular proteins in their native state are often modelled as compact polymers on a lattice (see [24] for a recent review).

Given this motivation, in this work we consider self-avoiding *dense* polymers with permanent entanglements, complementing our previous studies for the dilute phase [13,21]. A polymer is considered dense if, on a lattice, the fraction  $f$  of occupied sites has a finite value  $f > 0$ . This can be realised by a single polymer of total length  $L$  inside a box of volume  $V$  and taking the limit  $L \rightarrow \infty$ ,  $V \rightarrow \infty$  in such a way that  $f = L/V$  stays finite [25,26]. Alternatively, dense polymers can be obtained in an infinite volume through the action of an attractive force between monomers. Then, for temperatures  $T$  below the transition (Theta) temperature  $\Theta$ , the polymers collapse to a dense phase, with a density  $f > 0$ , which is a function of  $T$  [26,27]. For a dense polymer in  $d$  dimensions, the exponent  $\nu$ , defined by the radius of gyration  $R_g \sim L^\nu$ , is simply  $\nu = 1/d$ . In 2D, the dense polymer phase for  $0 < f < 1$  is related to a conformal field theory, and the resulting scaling behaviour is known exactly [25,26,28]. The limit  $f = 1$  is realised in Hamiltonian paths, where a random walk visits every site of a given lattice exactly once. For some cases, their scaling behaviour is known exactly as well [29,30]. Another way to make polymers collapse in 2D is to exert a pressure on self-avoiding loops (2D vesicles), conjugate to their area, which results in double-walled, branched structures [31,32]. Recently, the corresponding crossover scaling function from linear to branched polymers (lattice animals) has been obtained exactly [33]. It is believed that the branched and dense polymer phases are different.

Here, we extend our previous scaling analysis of knots in dilute polymers [13] to the dense phase, and at the  $\Theta$ -point. The general conclusion is that the entropic mechanism for tightening of entanglements is considerably weaker in the denser regimes. While the simple figure-eight structure is still tight in these phases, the trefoil becomes loose, with the trends more pronounced in the dense phase. Note that at the  $\Theta$ -point in 2D, the swelling exponent is  $\nu = 4/7$ , implying a fractal dimension  $1/\nu$  smaller than  $d = 2$ , and an asymptotic density of  $f = 0$ . In a recent numerical study, Orlandini, Stella, and Vanderzande [34] (hereafter referred to as OSV) investigate the tightness of the 2D projection of the trefoil knot, and find *delocalisation*, in contrast to the strong localisation obtained in the dilute case [13].

The main focus of this work is thus the localisation of flat entangled polymers in the dense phase and at the  $\Theta$ -point by means of scaling arguments, in analogy to the dilute case [13]. When possible, we compare these results with our own numerical simulations, as well as those by OSV. In Section 2 we first review the differentiation be-

tween tight (localised) and loose (delocalised) segments in entangled polymers. In Section 3 we then consider the 2D figure-eight structure (F8) and compare our scaling results with Monte Carlo simulations. In Section 4 we derive the scaling results for the 2D projection of the trefoil, and compare them with the simulations by OSV. Section 5 contains our conclusions. In Appendix A we compile some scaling results for general polymer networks. Finally, at the end of Appendix A, we consider briefly a newly discovered phase of 2D dense polymers where the strict non-crossing condition is relaxed [28].

## 2 Tight and loose segments

Consider an entangled polymer chain in 2D of length  $L$ , such as a simple flat, once-twisted ring with one crossing (called “figure-eight” (F8), see position III in Figure 1 top row) or the 2D projection of the trefoil pressed flat against a surface by an external force (Fig. 1) [11]. The orientations of the crossings are irrelevant, and can thus be considered as vertices with 4 outgoing legs. Thus, each structure is mapped on a 2D polymer network with a number of vertices which are joined by  $\mathcal{N}$  segments of variable lengths  $\{s_i\}$  under the constraint  $\sum_{i=1}^{\mathcal{N}} s_i = L$ . In the following we shall use the convention  $s_1 \leq s_2 \leq \dots \leq s_{\mathcal{N}}$ .

Since we are interested in the tightness of such a network, we define the size of the entangled region as  $\ell = \sum_{i=1}^{\mathcal{N}-1} s_i$  so that the remaining (largest) segment is  $s_{\mathcal{N}} = L - \ell$ . Clearly, for the F8,  $\mathcal{N} = 2$  and  $\ell = s_1$ , while for the trefoil  $\mathcal{N} = 6$  and  $\ell = \sum_{i=1}^5 s_i$ . Note that the above definition does not necessarily imply that  $\ell$  is small; however, if  $\ell \ll L$ , the structure assumes the form of a possibly multiply connected knot region of size  $\ell$  and a large simple loop of size  $L - \ell$ . For a knot represented by the network  $\mathcal{G}$ , an important quantity is its number of configurations  $\omega_{\mathcal{G}}(\ell, L)$  for fixed  $\ell$ . In general, in the tight limit  $\ell \ll L$ , the configuration number scales as a power law:

$$\omega_{\mathcal{G}}(\ell, L) \sim \ell^{-c_{\mathcal{G}}} \quad (\ell \ll L), \quad (1)$$

where the exponent  $c_{\mathcal{G}}$  depends on the topology of the network  $\mathcal{G}$ <sup>1</sup>.

For given  $\omega(\ell, L)$ , various quantities of interest can be calculated. For example, the mean size of the knot region is given by<sup>2</sup>

$$\langle \ell \rangle = \int_a^{L/2} d\ell \ell p(\ell, L), \quad (2)$$

with the (normalised) probability density function (PDF)

$$p(\ell, L) = \omega(\ell, L) / \int_a^{L/2} d\ell \omega(\ell, L). \quad (3)$$

<sup>1</sup> In the remainder of this section, we drop the index  $\mathcal{G}$  for ease of notation.

<sup>2</sup> The upper integration limit can be chosen as any finite fraction of  $L$  in principle; the choice of  $L/2$  imposes no restriction on generality.

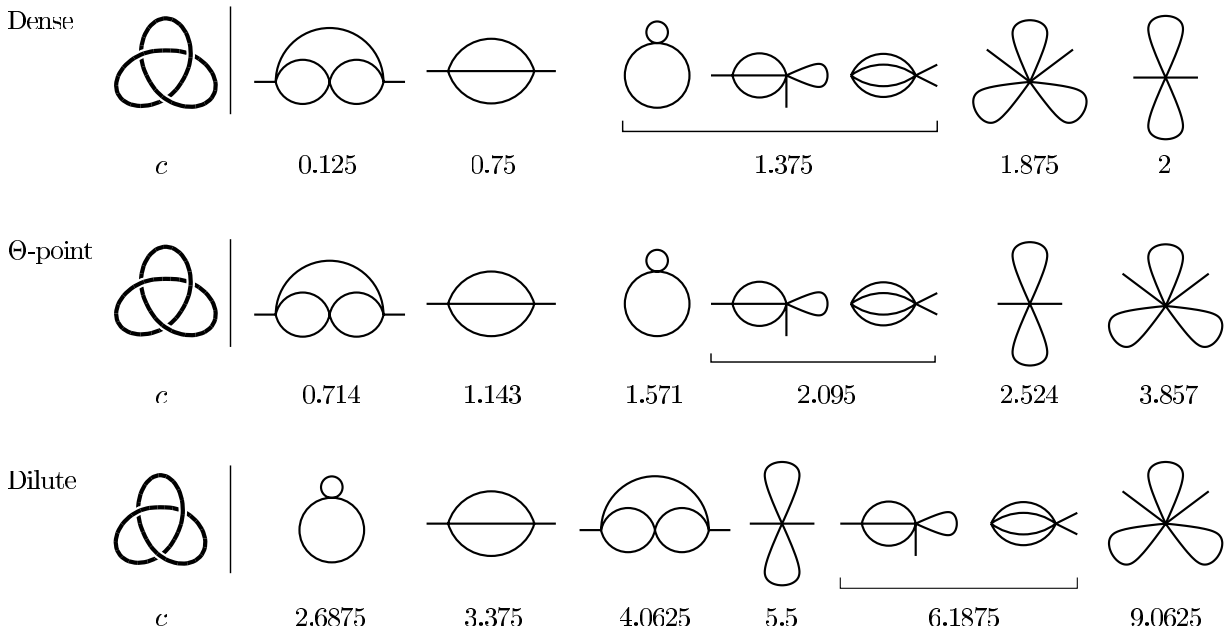


**Fig. 1.** “Contractions” of the flat trefoil knot, arranged according to higher scaling orders. The protruding legs stand for the remaining simply connected ring. Below the contractions, we list the associated scaling exponent  $c$  (see text). Both for dense polymers and polymers at the  $\Theta$ -point, the leading shape is the original (uncontracted) trefoil configuration on the very left. For comparison, we also show the corresponding ordering for the dilute phase [13].

We have introduced a short-distance cutoff  $a$ , set by the lattice constant, to control the non-integrable singularity at  $\ell = 0$  which occurs in equation (2) for  $c > 2$ , and in the denominator of equation (3) for  $c > 1$ . Thus, depending on the value of  $c$ , three cases can be distinguished:

- i)  $c < 1$ : Both integrals are well-defined for  $a = 0$ , and one immediately obtains  $\langle \ell \rangle \sim L$  due to dimensional considerations. The knot region grows linearly with  $L$  and is thus *delocalised*, *i.e.* spanning the whole polymer.
- ii)  $1 < c < 2$ : To leading order in  $a$ , one finds  $\langle \ell \rangle \sim a^{c-1} L^{2-c}$ . The size of the knot region scales with  $L$ , but with an exponent  $2 - c < 1$ , and is thus *weakly localised*, *i.e.*,  $\langle \ell \rangle / L \rightarrow 0$  for  $L \rightarrow \infty$ .
- iii)  $c > 2$ : To leading order in  $a$ , one finds  $\langle \ell \rangle \sim a$ , *i.e.*, the size of the knot region is independent of  $L$  for  $L \rightarrow \infty$ , and is thus *strongly localised*.

In a more complicated network, such as for the trefoil in Figure 1, several segments can be simultaneously tight. We shall refer to the emerging structures as possible *shapes* (or *contractions*) of the original network. Each shape corresponds again to a network  $\mathcal{G}$ . The parameter  $c$  not only determines the tightness of the knot region for given shape  $\mathcal{G}$ , but also controls the *overall likelihood*  $P_{\mathcal{G}}$ , of different possible shapes. The latter is obtained (up to normalisation) by integrating  $\omega_{\mathcal{G}}(\ell, L)$  over all possible values of  $\ell$ , as in the denominator of equation (3). Depending on the values of  $c$ , different cases can be distinguished:

- i)  $c < 1$ : The integral is convergent for small  $\ell$  with a finite limit for  $a \rightarrow 0$ , and scales as  $(a/L)^{c-1}$ . If there is a variety of shapes with  $c < 1$ , the one with the lowest value  $c_m$  is the most likely,  $P_{\mathcal{G}}$  for the others scaling

with a factor of  $(a/L)^{c-c_m}$ . This is expected, since networks with  $c < 1$  are delocalised over the whole chain of length  $L$ .

- ii)  $c > 1$ : The integral is divergent for small  $\ell$ , and is thus dominated by the lower cutoff. To make sure that the knot region is large enough to consider different vertices (crossings) as separated on a scale much larger than  $a$ , one should use a lower cutoff  $\mathcal{A}$  of intermediate length  $a \ll \mathcal{A} \ll L^3$ . The relative probabilities for different shapes with  $c > 1$  now scale with a factor of  $(a/\mathcal{A})^c$ . Different shapes with  $c > 1$  scale differently with the lower cutoff  $\mathcal{A}$ , but not differently with  $L$ . This reflects the fact that for  $c > 1$  the probability  $P_{\mathcal{G}}$  is dominated by the small  $\ell$  behaviour of  $\omega_{\mathcal{G}}(\ell, L)$ .

In both cases  $P_{\mathcal{G}}$  scales with a factor of  $a^c$ . This is the *scaling order* of such a shape  $\mathcal{G}$ , as the likelihood of possible shapes with distinct values of  $c$  can be ordered according to powers of  $a^c$  with more dominant networks for smaller values of  $c$  [13].

### 3 The 2D figure-eight: scaling analysis & simulations

The most elementary entangled object in 2D is the F8, which consists of two loops of variable lengths  $\ell$  and  $L - \ell$

<sup>3</sup> In a MC simulation, a larger  $\mathcal{A}$  gives worse statistics since configurations with  $\ell > \mathcal{A}$  become less frequent. In our case, we considered two vertices as separated if the segment between them was larger than 5 monomers. For the original trefoil this gives  $\mathcal{A} \approx 25$  monomer lengths (5 monomers  $\times$  5 segments).

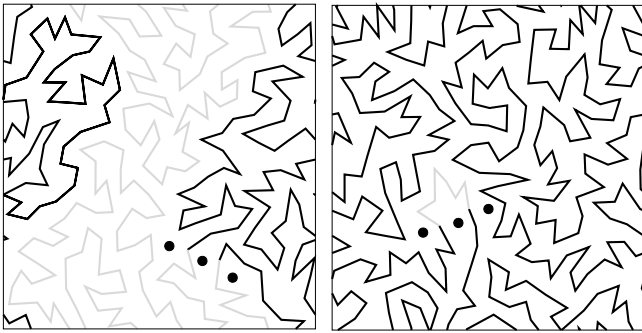


**Fig. 2.** Symmetric ( $\ell = L/2 = 128$ ) initial configuration of a 2D dense F8 (left), and its equilibrium configuration (right) with periodic boundary conditions. The slip-link is represented by the three (tethered) black dots.

(position III in Fig. 1 top row). The crossing point can be considered as a vertex with 4 outgoing legs, and the F8 corresponds to a network with  $\mathcal{N} = 2$  segments of lengths  $s_1 = \ell$  and  $s_2 = L - \ell$  [11]. The number of configurations  $\omega_8(\ell, L)$  for the F8 can be deduced from results for general polymer networks, obtained by Duplantier and coworkers [25,26,29,35], which are compiled in Appendix A. In 2D it has the scaling form

$$\omega_8(\ell, L) \sim \omega_0(L) (L - \ell)^{\gamma_8} \mathcal{X}\left(\frac{\ell}{L - \ell}\right). \quad (4)$$

As discussed in the previous section, the localisation of F8 is controlled by the limit of  $\omega_8(\ell, L)$  for  $\ell \rightarrow 0$ , *i.e.*, the behaviour of the scaling function  $\mathcal{X}(x)$  for  $x = \ell/(L - \ell) \rightarrow 0$ . The latter can be determined by the following argument (see text below Eq. (59) in Ref. [26]): Clearly, for  $\ell \ll L$ , the big loop of length  $L - \ell$  will behave like a simple ring, so that  $\omega_8(\ell, L)$  should reduce to  $\omega_0(L)$ . This implies  $\mathcal{X}(x) \sim x^{\gamma_8}$  as  $x \rightarrow 0$  and thus

$$\omega_8(\ell, L) \sim \omega_0(L) \ell^{-c} \quad (\ell \ll L). \quad (5)$$

The value of the exponent  $c$  for the 2D dense F8 (see App. A) is

$$c = -\gamma_8 = 11/8 = 1.375, \quad (6)$$

implying that the smaller loop is *weakly localised*. This means that the probability for the size of each loop is peaked at  $\ell = 0$  and, by symmetry, at  $\ell = L$ . An analogous reasoning for the 2D F8 at the  $\Theta$ -point gives

$$c = 11/7 = 1.571, \quad (7)$$

*i.e.*, in this case the smaller loop is also weakly localised.

Figure 2 shows the symmetric initial and a typical equilibrium configuration for periodic boundary conditions obtained from Monte Carlo (MC) simulations, see below for details. In Figure 2, the lines represent the bonds (tethers) between the monomers (beads, not shown here). The three black dots mark the locations of the tethered beads forming the slip-link in 2D, by which we model the crossing [13,21]. The initial symmetric configuration soon gives way to a configuration with  $\ell \ll L$  on approaching

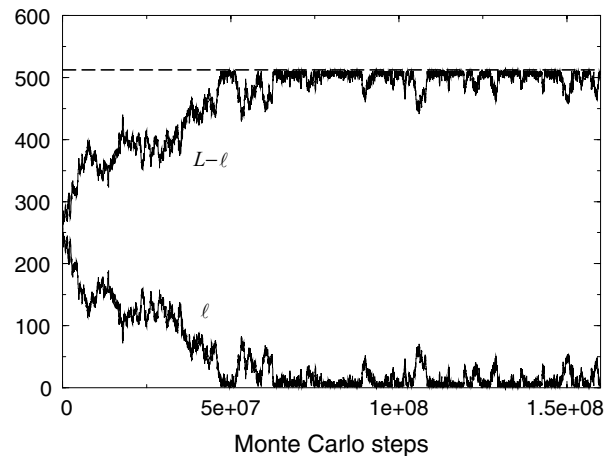


**Fig. 3.** The breaking of the initial symmetry between the two loops of the F8, as a function of MC steps at 55% area coverage.

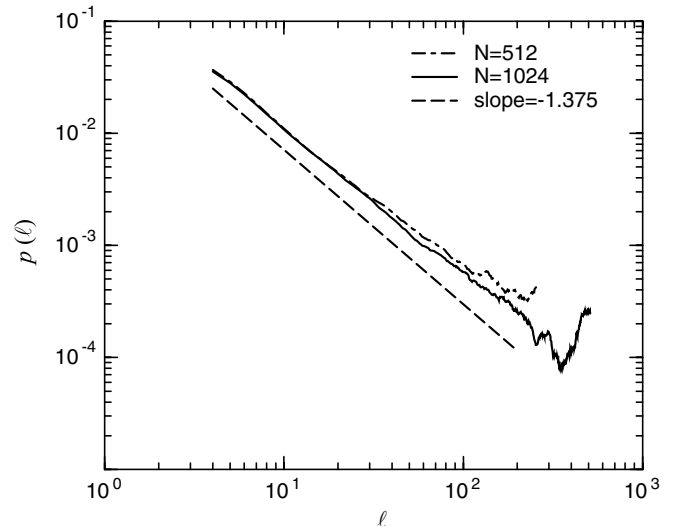


**Fig. 4.** The loop size probability distribution  $p(\ell)$  at  $\rho = 55\%$  area coverage, for the F8 with 512 (top line) and 1024 monomers (solid line). The power law with the predicted exponent  $c = 1.375$  in equation (6) is indicated by the dashed line.

equilibrium. Figure 3 shows the development of this symmetry breaking as a function of the number of MC steps. We note, however, that the fluctuations of the loop sizes in the “stationary” regime appear to be larger in comparison to the dilute case studied in reference [21]. We checked that for densities (area coverage) above 40% the scaling behaviour becomes independent of the density. The above simulation results correspond to a density of 55%, which is roughly half of the maximal possible density of 90% (closed-packed-area coverage). The size distribution data is well fitted to a power law (for over 1.5 decades with 1024 monomers), and the corresponding exponent with 512 and 1024 monomers in Figure 4 is in good agreement with the predicted value.

For our MC analysis, we used a hard-core bead-and-tether chain, in which self-crossings were prevented by keeping a maximum bead-to-bead distance of 1.9 times the bead diameter, and a maximum step length of 0.27 times the bead diameter (cf. also [11]). The slip-link was represented by three tethered beads enforcing the sliding pair contact such that the loops cannot fully retract, see Figure 2. To create the dense F8 initial condition, a free F8 is squeezed into a quadratic box with hard walls. This is achieved by starting off from the free F8, surrounding it by a box, and turning on a force directed towards one of the edges. Then, the opposite edge is moved towards the centre of the box, and so on. During these steps, the slip-link is locked, *i.e.*, the chain cannot slide through it, and the two loops are of equal length during the entire preparation. Finally, when the envisaged density is reached, the hard walls are replaced by periodic boundary conditions, and the slip-link is unlocked. For all densities studied we observe that one of the loops becomes much smaller than the other one. We consider the chain as relaxed when the structure has changed from symmetric ( $s_1 = s_2 = N/2$ ) to asymmetric ( $s_1 \sim 1$ ,  $s_2 \sim N$ ), then to symmetric and back again to asymmetric. After this we start to sample the probability distribution for the loop lengths. The probability distribution with chain length  $N = 1024$  and density  $\rho = 55\%$  required about  $3 \times 10^9$  Monte Carlo steps ( $\sim 3 \times 10^{12}$  attempted moves). We note that an explicit simulation to obtain the PDF  $p(\ell)$  for more complicated structures than the F8 was not possible within reasonable computation time with the MC algorithm we used.

#### 4 The 2D trefoil: scaling analysis & simulations

We now turn to the 2D projection of the trefoil (denoted “3”, cf. left part and position I in Fig. 1 top row). Each of the three crossings is replaced with a vertex of order four, resulting in a network with  $\mathcal{N} = 6$  segments of lengths  $\{s_i\}$  and total length  $L = \sum_{i=1}^6 s_i$  [11]. The size of the knot region is  $\ell = \sum_{i=1}^5 s_i$  and  $s_6 = L - \ell$ . According to Section 2, we need to know the behaviour of the configuration number  $\omega_3(\ell, L)$  for  $\ell \ll L$  in order to decide how  $\langle \ell \rangle$  scales with  $L$ . For *fixed* segment lengths  $\{s_i\}$  with  $\ell \ll L$ , the configuration number of the network can be derived by using equation (A.3) in Appendix A and an analogous reasoning invoked to obtain equation (5), resulting in

$$\omega'_3 \sim \omega_0(L) \ell^{\gamma_3} \mathcal{W}\left(\frac{s_1}{\ell}, \dots, \frac{s_4}{\ell}\right), \quad \ell \ll L. \quad (8)$$

The prime on  $\omega'_3$  indicates that the segment lengths  $\{s_i\}$  are fixed. However, since in our case the individual segments of the knot region may exchange length with each other and only the total length  $\ell$  of the knot region is fixed, we integrate  $\omega'_3$  over all distributions of lengths  $\{s_i\}$  under the constraint  $\ell = \sum_{i=1}^5 s_i$  [13]. This yields the desired number of configurations of the 2D trefoil with fixed  $\ell \ll L$  as

$$\omega_3(\ell, L) \sim \omega_0(L) \ell^{-c} \quad (9)$$

with  $c = -\gamma_3 - m$ , where  $\gamma_3 = -33/8$  from equation (A.2) in Appendix A ( $\mathcal{L} = 4$ ,  $n_4 = 3$ ) and  $m = 4$  is the number of independent integrations over chain segments. Thus,  $c = 1/8 < 1$  which implies that the dense 2D trefoil is *delocalised*.

The above analysis corresponds to the case for which all segments  $\{s_i\}$  are large compared with the short-distance cutoff  $a$ . Conversely, if some of the segments  $\{s_i\}$  are of the order of  $a$ , the vertices they join can no longer be resolved on macroscopic length scales, but constitute a new, single vertex, possibly with more than four outgoing legs. The corresponding *contractions* of the original 2D trefoil thus represent different networks, each one with its own topological exponent  $\gamma$  and localisation exponent  $c = -\gamma - m$  (where  $m$  is the number of independent integrations, see above). These contractions correspond to different *shapes*, which can be ordered according to their scaling order in  $a$ , *i.e.*, according to increasing powers of  $c$  (cf. Sect. 2).

For *dilute* polymers, we have shown in this way that the leading scaling order is the F8 with  $c = 43/16$ , and that the original (uncontracted) trefoil shape is only found at the third position [13]. For *dense* polymers, however, the present scaling results show that both the original trefoil shape ( $c = 1/8 < 1$ , see above) and position II ( $c = 3/4 < 1$ ) are in fact *delocalised* (top row in Fig. 1). The F8 is only found at the third position and is weakly localised ( $c = 11/8 > 1$ , cf. Sect. 3). Thus, in a MC simulation of the dense 2D trefoil, we predict that one mainly observes delocalised shapes corresponding to the original trefoil, and less frequently the other shapes of the hierarchy (top row) in Figure 1.

These predictions are consistent with the numerical simulations of Orlandini *et al.* [34] (OSV), who observe that the mean value of the second largest segment of the simulated 2D dense trefoil configurations grows linearly with  $L$ , and conjecture the same behaviour also for the other segments, corresponding to the delocalisation of the trefoil obtained above. However, we note that the configuration shown in Figure 1 of OSV corresponds in our modelling to the shape at position II in Figure 1, where we consider the two crossings to the right in Figure 1 of OSV as one “molten” vertex.

The same reasoning can be applied to the 2D trefoil in the  $\Theta$  phase. In this case we find that the leading shape is again the original (uncontracted) trefoil, with  $c = 5/7 < 1$ . This implies that the 2D trefoil is *delocalised* also at the  $\Theta$ -point. All other shapes are at least weakly localised, and subdominant to the leading scaling order represented by the original trefoil. The resulting hierarchy of shapes is shown in Figure 1 (middle row).

This finding is at variance with the simulation results of OSV at the  $\Theta$ -point, who observe a behaviour of the simulated trefoil configurations similar to the F8, which is weakly localised with  $c = 11/7 > 1$ , and is found only at the third position in the hierarchy of Figure 1.

## 5 Conclusions

We presented a scaling analysis for the 2D figure-eight structure (F8) and the 2D projection of the trefoil knot at equilibrium, both in the dense phase and at the  $\Theta$ -point [11]. Figure 1 shows the hierarchy of contractions of the original trefoil, arranged according to scaling order. The F8 structure represents the leading order of the hierarchy in the dilute phase [13], but does not play a special role in the other states. Thus we conclude that the 2D trefoil is *delocalised* both in the dense phase and at the  $\Theta$ -point, in contrast to its localisation in the dilute case [13]. The delocalisation of the flat trefoil in the dense phase has been observed in the simulations by Orlandini *et al.* [34] (OSV). However, their observation of behaviour corresponding to a weakly localised F8 at the  $\Theta$  transition contradicts our results.

If the chain's topology is that of a F8, then one of the loops is predicted to be tight in all cases, although the localisation exponent depends on the polymer phase. We explicitly verified the localisation exponent of  $c = 11/8$  by a MC study of a F8 in the dense phase. (We employed periodic boundary conditions for this simulations to avoid any potential problems associated with surface effects.)

In 2D, the scaling analysis can be readily extended to general prime knots. Indeed, the minimal 2D projection of any prime knot can be mapped on a network  $\mathcal{G}$ , for which one can calculate the corresponding exponent  $c$  in a similar way as before. Using the Euler relations  $2\mathcal{N} = \sum_{N \geq 1} N n_N$  and  $\mathcal{L} = \sum_{N \geq 1} \frac{1}{2}(N - 2)n_N + 1$ , we find

$$c_{\mathcal{G}} = 2 + \sum_{N \geq 4} n_N \left[ \frac{N}{2}(d\nu - 1) + (|\sigma_N| - d\nu) \right]. \quad (10)$$

Both for dense polymers and polymers at the  $\Theta$ -point in 2D one has  $d\nu \geq 1$  and  $|\sigma_N|$  increases with  $N$ , so that the term in the square brackets in the above expression increases with  $N$  as well. For a fixed number  $\mathcal{V} = \sum_{N \geq 4} n_N$  of vertices this implies that  $c_{\mathcal{G}}$  is minimal if only vertices with four outgoing legs are present. Using this and the fact that for  $N = 4$  the term in the square brackets is negative<sup>4</sup>, we conclude that  $c_{\mathcal{G}}$  is minimal if the number of such 4-vertices is maximal. This implies that the leading scaling order of the 2D projection of *any* prime knot is the original (uncontracted) configuration, for which the above vertices represent the crossings, and this configuration will be *delocalised* (since the 2D trefoil configuration is already delocalised).

We thank J. Cardy and U. Seifert for helpful discussions. This work was supported by the National Science Foundation (DMR-01-18213) and the US-Israel Binational Science Foundation (BSF) grant No. 1999-007. RM acknowledges partial support from the Deutsche Forschungsgemeinschaft.

<sup>4</sup> Conversely, for dilute polymers this bracket is positive. This is the reason why the order of the first 3 contractions in each row of Figure 1 (which have only vertices with four outgoing legs) for dilute polymers is reverse compared to dense and  $\Theta$  polymers.

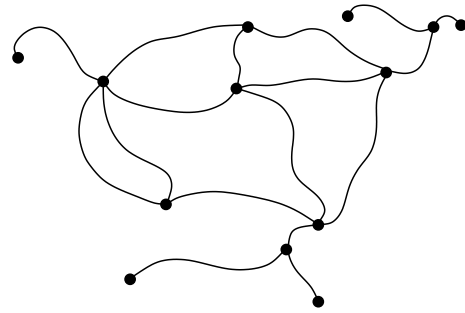


**Fig. 5.** Polymer network  $\mathcal{G}$  with vertices ( $\bullet$ ) of different order ( $n_1 = 5$ ,  $n_3 = 4$ ,  $n_4 = 3$ ,  $n_5 = 1$ ).

## Appendix A. Scaling in general polymer networks

In this appendix we review the scaling results for polymer networks in the dense phase in 2D [25–27, 29] and at the  $\Theta$  transition [35].

A general polymer network  $\mathcal{G}$ , like the one depicted in Figure 5, consists of a number of vertices which are joined by  $\mathcal{N}$  chain segments of total length  $L$ . First, consider the dense phase in 2D. If all segments have equal length  $s$  and  $L = \mathcal{N}s$ , the configuration number  $\omega_{\mathcal{G}}$  of such a network scales as [25, 26]<sup>5</sup>

$$\omega_{\mathcal{G}}(s) \sim \omega_0(L) s^{\gamma_{\mathcal{G}}}, \quad (A.1)$$

where  $\omega_0(L)$  is the configuration number of a simple ring of length  $L$ . For dense polymers, and in contrast to the dilute and  $\Theta$  phases,  $\omega_0(L)$  (and thus  $\omega_{\mathcal{G}}$ ) depends on the boundary conditions and even on the shape of the system [26, 27]. For example, for periodic boundary conditions (which we focus on in this study) corresponding to a 2D torus, one finds  $\omega_0(L) \sim \mu^L L^{\Psi-1}$  with a connectivity constant  $\mu$  and  $\Psi = 1$  [26]. However, the network exponent

$$\gamma_{\mathcal{G}} = 1 - \mathcal{L} + \sum_{N \geq 1} n_N \sigma_N \quad (A.2)$$

is *universal* and depends only on the topology of the network by the number  $\mathcal{L}$  of independent loops, and by the number  $n_N$  of vertices of order  $N$  with vertex exponents  $\sigma_N = (4 - N^2)/32$  [25, 26]. For a linear chain, the corresponding exponent  $\gamma_{\text{lin}} = 19/16$  has been verified by numerical simulations [26, 36]. For a network made up of different segment lengths  $\{s_i\}$  of total length  $L = \sum_{i=1}^{\mathcal{N}} s_i$ , equation (A.1) generalises to (cf. Sect. 4 in Ref. [26])

$$\omega_{\mathcal{G}}(s_1, \dots, s_{\mathcal{N}}) \sim \omega_0(L) s_{\mathcal{N}}^{\gamma_{\mathcal{G}}} \mathcal{Y}_{\mathcal{G}} \left( \frac{s_1}{s_{\mathcal{N}}}, \dots, \frac{s_{\mathcal{N}-1}}{s_{\mathcal{N}}} \right), \quad (A.3)$$

which involves the scaling function  $\mathcal{Y}_{\mathcal{G}}$ .

<sup>5</sup> Note that due to the factor  $\omega_0(L)$  the exponent of  $s$  is  $\gamma_{\mathcal{G}}$ , and not  $\gamma_{\mathcal{G}} - 1$  like in the expressions used in the dilute and  $\Theta$  phases, for which  $\omega_0(L) \sim L^{-d\nu}$ . However, for 2D dense polymers one has  $d\nu = 1$ , so that both definitions of  $\gamma_{\mathcal{G}}$  are equivalent, cf. Section 3 in reference [26].

For polymers in an infinite volume and endowed with an attractive interaction between neighbouring monomers, a different scaling behaviour emerges if the system is not below but right at the  $\Theta$ -point [35]. In this case the number of configurations of a general network  $\mathcal{G}$  is given by

$$\bar{\omega}_{\mathcal{G}}(s_1, \dots, s_N) \sim \mu^L s_N^{\bar{\gamma}_{\mathcal{G}}-1} \bar{\mathcal{Y}}_{\mathcal{G}} \left( \frac{s_1}{s_N}, \dots, \frac{s_{N-1}}{s_N} \right), \quad (\text{A.4})$$

with the network exponent

$$\bar{\gamma}_{\mathcal{G}} = 1 - d\nu\mathcal{L} + \sum_{N \geq 1} n_N \bar{\sigma}_N. \quad (\text{A.5})$$

Overlined symbols refer to polymers at the  $\Theta$ -point. In  $d = 2$ ,  $\nu = 4/7$  and  $\bar{\sigma}_N = (2 - N)(2N + 1)/42$  [35].

Finally, we note that equation (A.2) with  $\sigma_N = (4 - N^2)/32$  holds for a 2D dense polymer network which never intersects (apart from the vertices). However, it has been shown recently that a *different*, so-called ‘‘Goldstone phase’’ emerges if the strict non-crossing condition is relaxed; *i.e.*, if crossings *are* allowed albeit, disfavoured [28]. It is argued in reference [28] that in this case the scaling dimensions  $X_k$  of the so-called  $k$ -leg operators all vanish. This implies  $\sigma_N = 0$  in equation (A.2) (see Eq. (13) in [25] and the Euler relations near Eq. (10) above), *i.e.*, the asymptotic behavior is similar to a network of chains without self-avoiding constraints (ideal polymers). The localisation exponent  $c$  is then simply given by  $c = -\gamma_{\mathcal{G}} - m = \mathcal{L} - m - 1$ , resulting in  $c$  values of  $-1, 0, 1, 0, 0, 1, 1$  for the 7 contractions shown in Figure 1, top row from left to right. As argued before, all contractions with  $c < 1$  are delocalised; in particular the original (uncontracted) trefoil shape, is the dominant form with the smallest  $c$ . Our finding for the 2D dense phase in Section 4 is thus also applicable in the Goldstone phase. However, in a MC simulation of the Goldstone phase it will be hard to identify the knot, as additional crossings are allowed and will occur.

## References

1. P.-G. de Gennes, *Scaling Concepts in Polymer Physics* (Cornell University Press, Ithaca, New York, 1979).
2. M. Doi, S.F. Edwards, *The Theory of Polymer Dynamics* (Clarendon Press, Oxford, 1986).
3. J.D. Ferry, *Viscoelastic Properties of Polymers* (Wiley, New York, 1970).
4. L.R.G. Treloar, *The Physics of Rubber Elasticity* (Clarendon Press, Oxford, 1975).
5. J.P. Sauvage, C. Dietrich-Buchecker (Editors), *Catenanes, Rotaxanes, and Knots* (VCH, Weinheim, 1999).
6. T.E. Creighton, *Proteins: Structures and Molecular Properties* (W.H. Freeman, New York, 1993).
7. B. Alberts, A. Johnson, J. Lewis, M. Raff, K. Roberts, P. Walter, *Molecular Biology of the Cell* (Garland, New York, 2002).
8. V.V. Rybenkov *et al.*, *Science* **277**, 690 (1997); J. Yan, M.O. Magnasco, J.F. Marko, *Nature* **401**, 932 (1999); A.V. Vologodskii *et al.*, *Proc. Natl. Acad. Sci. U.S.A.* **98**, 3045 (2001).
9. W.E. Moerner, M. Orrit, *Science* **283**, 1670 (1999); M.C. Williams, I. Rouzina, V.A. Bloomfield, *Acc. Chem. Res.* **35**, 159 (2002).
10. A.D. Mehta, M. Rief, J.A. Spudich, D.A. Smith, R.M. Simmons, *Science* **283**, 1689 (1999); A. van Oudenaarden, J.A. Theriot, *Nat. Cell. Biol.* **1**, 493 (1999).
11. Throughout this paper we employ the terms ‘‘2D knot,’’ ‘‘2D knot projection,’’ and ‘‘2D network’’ to denote a polymer chain confined to two dimensions, which never intersects itself apart from explicitly imposed ‘‘crossings’’ (or ‘‘vertices’’). The chain segments adjoining the crossings are allowed to exchange length with one another. Also the slip-linked structures considered in Sections 3 and 4 belong to this class of systems, as their equilibrium behaviour is the same. The strict non-crossing condition is relaxed only briefly near the end of Appendix A, where we consider the 2D Goldstone phase introduced in reference [28].
12. E. Guitter, E. Orlandini, *J. Phys. A* **32**, 1359 (1999).
13. R. Metzler, A. Hanke, P.G. Dommersnes, Y. Kantor, M. Kardar, *Phys. Rev. Lett.* **88**, 188101 (2002).
14. B. Duplantier, *Phys. Rev. Lett.* **57**, 941 (1986); *J. Stat. Phys.* **54**, 581 (1989).
15. K. Ohno, K. Binder, *J. Phys. (Paris)* **49**, 1329 (1988); L. Schäfer *et al.*, *Nucl. Phys. B* **374**, 473 (1992).
16. M.B. Hastings, Z.A. Daya, E. Ben-Naim, R.E. Ecke, *Phys. Rev. E* **66**, 025102 (2002).
17. B. Maier, J.O. Rädler, *Phys. Rev. Lett.* **82**, 1911 (1999); B. Maier, U. Seifert, J.O. Rädler, *Europhys. Lett.* **60**, 622 (2002).
18. A.Yu. Grosberg, A.R. Khokhlov, *Statistical Physics of Macromolecules* (AIP Press, New York, 1994).
19. J.D. Moroz, R.D. Kamien, *Nucl. Phys. B* **506**, 695 (1997); W. Kung, R.D. Kamien, *cond-mat/0305026*.
20. E.J. Janse van Rensburg, S.G. Whittington, *J. Phys. A* **24**, 3935 (1991); E. Orlandini, M.C. Tesi, E.J. Janse van Rensburg, S.G. Whittington, *J. Phys. A* **31**, 5953 (1998); **29**, L299 (1996); V. Katritch, W.K. Olson, A. Vologodskii, J. Dubochet, A. Stasiak, *Phys. Rev. E* **61**, 5545 (2000); M.K. Shimamura, T. Deguchi, *Phys. Rev. E* **64**, 020801 (2001).
21. R. Metzler, A. Hanke, P.G. Dommersnes, Y. Kantor, M. Kardar, *Phys. Rev. E* **65**, 061103 (2002).
22. S.R. Quake, *Phys. Rev. Lett.* **73**, 3317 (1994); A.Yu. Grosberg, A. Feigel, Y. Rabin, *Phys. Rev. E* **54**, 6618 (1996); A.Yu. Grosberg, *Phys. Rev. Lett.* **85**, 3858 (2000); R. Metzler, *New J. Phys.* **4**, 91 (2002).
23. V.A. Bloomfield, *Biopolymers* **44**, 269 (1997); V.V. Vasilevskaya, A.R. Khokhlov, Y. Matsuzawa, K. Yoshikawa, *J. Chem. Phys.* **102**, 6595 (1995); L. Lerman, *Proc. Natl. Acad. Sci. U.S.A.* **68**, 1886 (1971); see also H. Walter, D.E. Brooks, *FEBS Lett.* **361**, 135 (1995) and references therein.
24. T. Garel, *Remarks on homo- and hetero-polymeric aspects of protein folding*, *cond-mat/0305053*.
25. B. Duplantier, *J. Phys. A* **19**, L1009 (1986).
26. B. Duplantier, H. Saleur, *Nucl. Phys. B* **290**, 291 (1987).
27. A.L. Owczarek, T. Prellberg, R. Brak, *Phys. Rev. Lett.* **70**, 951 (1993); B. Duplantier, *Phys. Rev. Lett.* **71**, 4274 (1993); A.L. Owczarek, T. Prellberg, R. Brak, *Phys. Rev. Lett.* **71**, 4275 (1993).
28. J.L. Jacobsen, N. Read, H. Saleur, *Phys. Rev. Lett.* **90**, 090601 (2003).
29. B. Duplantier, F. David, *J. Stat. Phys.* **51**, 327 (1988).

30. J. Kondev, J.L. Jacobsen, Phys. Rev. Lett. **81**, 2922 (1998).
31. M.E. Fisher, Physica D **38**, 112 (1989).
32. E. Orlandini, F. Seno, A.L. Stella, M.C. Tesi, Phys. Rev. Lett. **68**, 488 (1992); R. Dekeyser, E. Orlandini, A.L. Stella, M.C. Tesi, Phys. Rev. E **52**, 5214 (1995).
33. J. Cardy, J. Phys. A **34**, L665 (2001).
34. E. Orlandini, A.L. Stella, C. Vanderzande, Phys. Rev. E **68**, 031804 (2003).
35. B. Duplantier, H. Saleur, Phys. Rev. Lett. **59**, 539 (1987).
36. P. Grassberger, R. Hegger, Ann. Phys. (Leipzig) **4**, 230 (1995).